nature materials

REVIEW ARTICLE

PUBLISHED ONLINE: 19 FEBRUARY 2010 | DOI: 10.1038/NMAT2629

Plasmonics for improved photovoltaic devices

Harry A. Atwater[1]* and Albert Polman[2]*

The emerging field of plasmonics has yielded methods for guiding and localizing light at the nanoscale, well below the scale of the wavelength of light in free space. Now plasmonics researchers are turning their attention to photovoltaics, where design approaches based on plasmonics can be used to improve absorption in photovoltaic devices, permitting a considerable reduction in the physical thickness of solar photovoltaic absorber layers, and yielding new options for solar-cell design. In this review, we survey recent advances at the intersection of plasmonics and photovoltaics and offer an outlook on the future of solar cells based on these principles.

Photovoltaics, the conversion of sunlight to electricity, is a promising technology that may allow the generation of electrical power on a very large scale. Worldwide photovoltaic production was more than 5 GW in 2008, and is expected to rise above 20 GW by 2015. Photovoltaics could thus make a considerable contribution to solving the energy problem that our society faces in the next generation. To make power from photovoltaics competitive with fossil-fuel technologies, the cost needs to be reduced by a factor of 2–5. At present most of the solar-cell market is based on crystalline silicon wafers with thicknesses between 180–300 μm, and most of the price of solar cells is due to the costs of silicon materials and processing. Because of this, there is great interest in thin-film solar cells, with film thicknesses in the range 1–2 μm, that can be deposited on cheap module-sized substrates such as glass, plastic or stainless steel. Thin-film solar cells are made from a variety of semiconductors including amorphous and polycrystalline Si, GaAs, CdTe and $CuInSe_2$, as well as organic semiconductors. A limitation in all thin-film solar-cell technologies is that the absorbance of near-bandgap light is small, in particular for the indirect-bandgap semiconductor Si. Therefore, structuring the thin-film solar cell so that light is trapped inside to increase the absorbance is very important. A significant reduction in thin-film solar-cell thickness would also allow the large-scale use of scarce semiconductor materials such as In and Te that are available in the Earth's crust in only small quantities.

In conventional thick Si solar cells, light trapping is typically achieved using a pyramidal surface texture that causes scattering of light into the solar cell over a large angular range, thereby increasing the effective path length in the cell[1–3]. Such large-scale geometries are not suitable for thin-film cells, for geometrical reasons (as the surface roughness would exceed the film thickness) and because the greater surface area increases minority carrier recombination in the surface and junction regions.

A new method for achieving light trapping in thin-film solar cells is the use of metallic nanostructures that support surface plasmons: excitations of the conduction electrons at the interface between a metal and a dielectric. By proper engineering of these metallodielectric structures, light can be concentrated and 'folded' into a thin semiconductor layer, thereby increasing the absorption. Both localized surface plasmons excited in metal nanoparticles and surface plasmon polaritons (SPPs) propagating at the metal/semiconductor interface are of interest.

In the past few years, the field of plasmonics has emerged as a rapidly expanding new area for materials and device research[4]. This is a result of the large array of tools that have become available for nanoscale fabrication and nanophotonics characterization, and also because of the availability of powerful electromagnetic simulation methods that are critical to understanding and harnessing plasmon excitations. Studies are just starting to appear illustrating the coupling of plasmons to optical emitters[5–7]; plasmon focusing[8,9]; hybridized plasmonic modes in nanoscale metal shells[10]; nanoscale waveguiding[11–14]; nanoscale optical antennas[15]; plasmonic integrated circuits[16,17]; nanoscale switches[18]; plasmonic lasers[19–21]; surface-plasmon-enhanced light-emitting diodes[22]; imaging below the diffraction limit[23]; and materials with negative refractive index[24–26]. Despite all these exciting opportunities, until recently little systematic thought has been given to the question of how plasmon excitation and light localization might be used advantageously in high-efficiency photovoltaics.

Plasmonics for photovoltaics

Conventionally, photovoltaic absorbers must be 'optically thick' to allow near-complete light absorption and photocarrier current collection. Figure 1a shows the standard AM1.5 solar spectrum together with a graph that illustrates what fraction of the solar spectrum is absorbed on a single pass through a 2-μm-thick crystalline Si film. Clearly, a large fraction of the solar spectrum, in particular in the intense 600–1,100 nm spectral range, is poorly absorbed. This is the reason that, for example, conventional wafer-based crystalline Si solar cells have a much larger thickness of typically 180–300 μm. But high-efficiency solar cells must have minority carrier diffusion lengths several times the material thickness for all photocarriers to be collected (see Fig. 1b), a requirement that is most easily met for thin cells. Solar-cell design and materials-synthesis considerations are strongly dictated by these opposing requirements for optical absorption thickness and carrier collection length.

Plasmonic structures can offer at least three ways of reducing the physical thickness of the photovoltaic absorber layers while keeping their optical thickness constant. First, metallic nanoparticles can be used as subwavelength scattering elements to couple and trap freely propagating plane waves from the Sun into an absorbing semiconductor thin film, by folding the light into a thin absorber layer (Fig. 2a). Second, metallic nanoparticles can be used as subwavelength antennas in which the plasmonic near-field is coupled to the semiconductor, increasing its effective absorption cross-section (Fig. 2b). Third, a corrugated metallic film on the back surface of a thin photovoltaic absorber layer can couple sunlight into SPP modes supported at the metal/semiconductor interface as well as

[1]Caltech Center for Sustainable Energy Research and Thomas J. Watson Laboratories of Applied Physics, California Institute of Technology, Pasadena, California 91125, USA. [2]Center for Nanophotonics, FOM Institute AMOLF, Science Park 104, 1098 XG Amsterdam, The Netherlands.
*e-mail: haa@caltech.edu; polman@amolf.nl

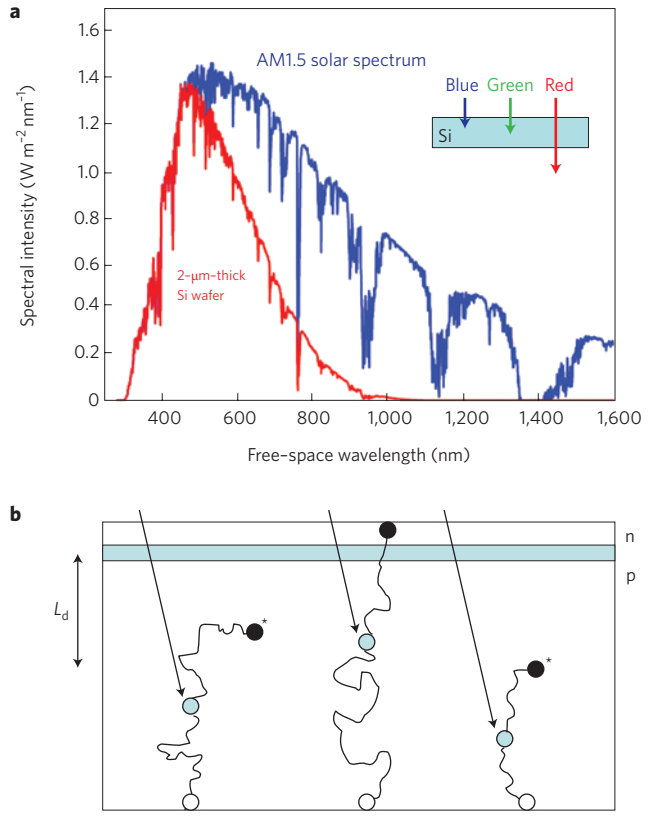

Figure 1 | Optical absorption and carrier diffusion requirements in a solar cell. a, AM1.5 solar spectrum, together with a graph that indicates the solar energy absorbed in a 2-μm-thick crystalline Si film (assuming single-pass absorption and no reflection). Clearly, a large fraction of the incident light in the spectral range 600–1,100 nm is not absorbed in a thin crystalline Si solar cell. **b**, Schematic indicating carrier diffusion from the region where photocarriers are generated to the p–n junction. Charge carriers generated far away (more than the diffusion length L_d) from the p–n junction are not effectively collected, owing to bulk recombination (indicated by the asterisk).

guided modes in the semiconductor slab, whereupon the light is converted to photocarriers in the semiconductor (Fig. 2c).

As will be discussed in detail in the next section, these three light-trapping techniques may allow considerable shrinkage (possibly 10- to 100-fold) of the photovoltaic layer thickness, while keeping the optical absorption (and thus efficiency) constant. Various additional ways of using plasmonic nanostructures to increase photovoltaic energy conversion are described in the section on other plasmonic solar-cell designs.

Plasmonic light trapping in thin-film solar cells

Light scattering using particle plasmons. Light scattering from a small metal nanoparticle embedded in a homogeneous medium is nearly symmetric in the forward and reverse directions[27,28]. This situation changes when the particle is placed close to the interface between two dielectrics, in which case light will scatter preferentially into the dielectric with the larger permittivity[29]. The scattered light will then acquire an angular spread in the dielectric that effectively increases the optical path length (see Fig. 2a). Moreover, light scattered at an angle beyond the critical angle for reflection (16° for the Si/air interface) will remain trapped in the cell. In addition, if the cell has a reflecting metal back contact, light reflected towards the surface will couple to the nanoparticles and be partly reradiated into the wafer by the same scattering mechanism. As a result, the incident light will pass several times through the semiconductor film, increasing the effective path length.

The enhanced incoupling of light into semiconductor thin films by scattering from plasmonic nanoparticles was first recognized by Stuart and Hall, who used dense nanoparticle arrays as resonant scatterers to couple light into Si-on-insulator photodetector structures[30,31]. They observed a roughly 20-fold increase in the infrared photocurrent in such a structure. This research field then remained relatively dormant for many years, until applications in thin-film solar cells emerged, with papers published on enhanced light coupling into single-crystalline Si (ref. 32), amorphous Si (refs 33,34), Si-on-insulator[35], quantum well[36] and GaAs (ref. 37) solar cells covered with metal nanoparticles.

Although there is now considerable experimental evidence that light scattering from metal nanoparticle arrays increases the photocurrent spectral response of thin-film solar cells, many of the underlying physical mechanisms and their interplay have not been studied systematically. The full potential of the particle scattering concept, taking into account integration with optimized anti-reflection coatings, is being studied by several research groups. In recent papers[38,39], we reported that both shape and size of metal nanoparticles are key factors determining the incoupling efficiency. This is illustrated in Fig. 3a, which shows that smaller particles, with their effective dipole moment located closer to the semiconductor layer, couple a larger fraction of the incident light into the underlying semiconductor because of enhanced near-field coupling. Indeed, in the limit of a point dipole very near to a silicon substrate, 96% of the incident light is scattered into the substrate, demonstrating the power of

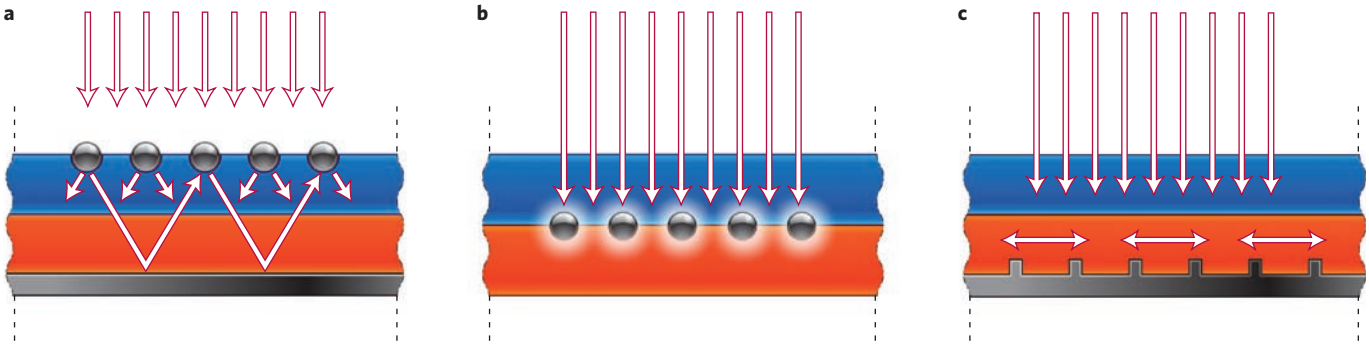

Figure 2 | Plasmonic light-trapping geometries for thin-film solar cells. a, Light trapping by scattering from metal nanoparticles at the surface of the solar cell. Light is preferentially scattered and trapped into the semiconductor thin film by multiple and high-angle scattering, causing an increase in the effective optical path length in the cell. **b**, Light trapping by the excitation of localized surface plasmons in metal nanoparticles embedded in the semiconductor. The excited particles' near-field causes the creation of electron–hole pairs in the semiconductor. **c**, Light trapping by the excitation of surface plasmon polaritons at the metal/semiconductor interface. A corrugated metal back surface couples light to surface plasmon polariton or photonic modes that propagate in the plane of the semiconductor layer.

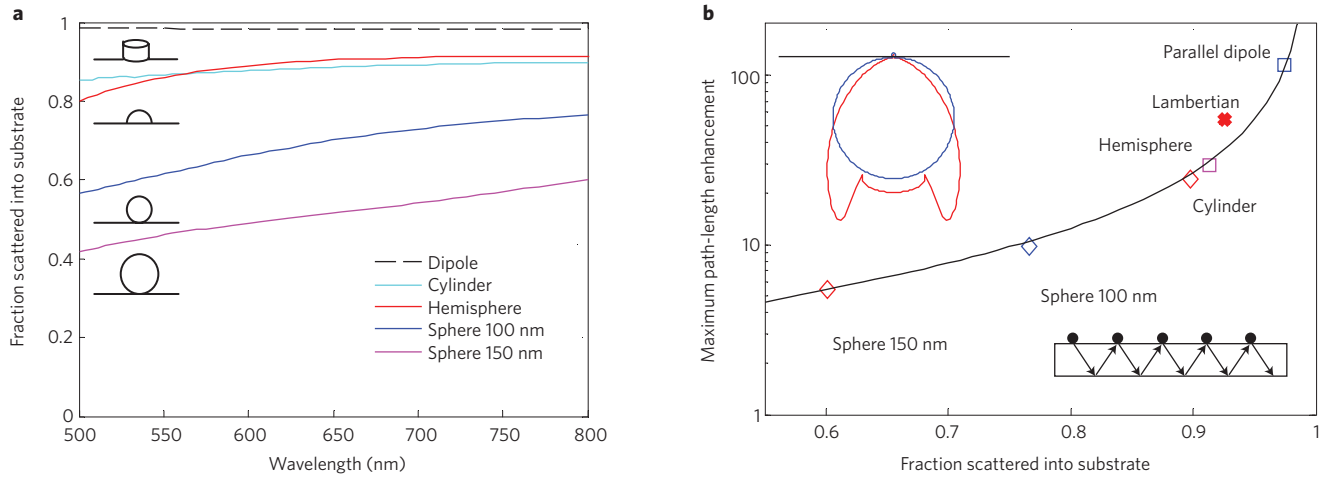

Figure 3 | Light scattering and trapping is very sensitive to particle shape. a, Fraction of light scattered into the substrate, divided by total scattered power, for different sizes and shapes of Ag particles on Si. Also plotted is the scattered fraction for a parallel electric dipole that is 10 nm from a Si substrate. **b**, Maximum path-length enhancement, according to a first-order geometrical model, for the same geometries as in **a** at a wavelength of 800 nm. Absorption within the particles is neglected for these calculations, and an ideal rear reflector is assumed. The line is a guide for the eye. Insets: (top left) angular distribution of scattered power for a parallel electric dipole that is 10 nm above a Si surface (red) and a Lambertian scatterer (blue); (lower right) geometry considered for calculating the path-length enhancement. Figure reproduced with permission: © 2008 AIP.

the particle scattering technique. Figure 3b shows the path-length enhancement in the solar cell derived from Fig. 3a using a simple first-order scattering model. For 100-nm-diameter Ag hemispheres on Si, a 30-fold enhancement is found. These light-trapping effects are most pronounced at the peak of the plasmon resonance spectrum, which can be tuned by engineering the dielectric constant of the surrounding matrix. For example, small Ag or Au particles in air have plasmon resonances at 350 nm and 480 nm respectively; they can be redshifted in a controlled way over the entire 500–1,500 nm spectral range by (partially) embedding them in SiO_2, Si_3N_4 or Si (refs 40–42; Fig. 4a), which are all standard materials in solar-cell manufacturing. A dielectric spacer layer between the nanoparticles and the semiconductor also causes electrical isolation, thereby avoiding additional surface recombination owing to the presence of the metal. The scattering cross-sections for metal nanoparticle scattering can be as high as ten times the geometrical area[28,38], and a ~10% coverage of the solar cell would thus suffice to capture most of the incident sunlight into plasmon excitations.

Optimization of plasmonic light trapping in a solar cell is a balancing act in which several physical parameters must be taken into account. First of all, Fig. 3 demonstrates the advantage of using small particles to create the forward scattering anisotropy. But very small particles suffer from significant ohmic losses, which scale with volume v, whereas scattering scales with v^2, so that using larger particles is advantageous to increase the scattering rate. For example, a 150-nm-diameter Ag particle in air has an albedo (fraction of light emitted as radiation) as large as 95%. Interestingly, the effective scattering cross-section can be increased by spacing the particles further away from the substrate, as this avoids destructive interference effects between the incident and reflected fields, albeit at the price of reduced near-field coupling[38,39]. For frequencies above the plasmon resonance, Fano resonance effects can cause destructive interference between scattered and unscattered light beams, and thus can cause reflection rather than enhanced incoupling[42,43]. One way to overcome the latter problem is by using a geometry in which particles are placed on the rear of the solar cell[42,44]. In this case, blue and green light is directly absorbed in the cell, whereas poorly absorbed (infra-)red light is scattered and trapped using metal nanoparticles. Similarly, light may be coupled in by using arrays of metal strips placed on the solar-cell surface. Calculations show that using this geometry can enhance the short-circuit current by 45% compared with a solar cell with a flat back contact[45]. Finally, in designing optimized plasmonic light-trapping arrays, we must take into account coupling between the nanoparticles, ohmic damping, grating diffraction effects[46] and the coupling to waveguide modes[47–49].

Light concentration using particle plasmons. An alternative use of resonant plasmon excitation in thin-film solar cells is to take advantage of the strong local field enhancement around the metal nanoparticles to increase absorption in a surrounding semiconductor material. The nanoparticles then act as an effective 'antenna' for the incident sunlight that stores the incident energy in a localized surface plasmon mode (Fig. 4b). This works particularly well for small (5–20 nm diameter) particles for which the albedo is low. These antennas are particularly useful in materials where the carrier diffusion lengths are small, and photocarriers must thus be generated close to the collection junction area. For these antenna energy conversion effects to be efficient, the absorption rate in the semiconductor must be larger than the reciprocal of the typical plasmon decay time (lifetime ~10–50 fs), as otherwise the absorbed energy is dissipated into ohmic damping in the metal. Such high absorption rates are achievable in many organic and direct-bandgap inorganic semiconductors.

Several examples of this concept have recently appeared that demonstrate enhanced photocurrents owing to the plasmonic near-field coupling. Enhanced efficiencies have been demonstrated for ultrathin-film organic solar cells doped with very small (5 nm diameter) Ag nanoparticles[50]. Plasmon-enhanced organic solar cells have also been demonstrated using electrodeposited Ag (ref. 51). An increase in efficiency by a factor of 1.7 has been shown for organic bulk heterojunction solar cells[52,53]. Dye-sensitized solar cells can also be enhanced by embedding small metal nanoparticles, as reported elsewhere[54–56]. Also, inorganic solar cells have shown increased photocurrents owing to near-field effects, such as CdSe/Si heterostructures[57]. Work on increased light absorption by metal nanoparticles embedded in Si has also been reported[58,59]. More recently, the coupling between plasmons in arrays of metal nanoparticles has been used to engineer the field enhancement to overlap with a selected area of the junction[53]. The dynamics (and optimization) of the coupling between plasmons, excitons and phonons in metal–semiconductor nanostructures is a rich field of research that so far has not received much attention with photovoltaics in mind.

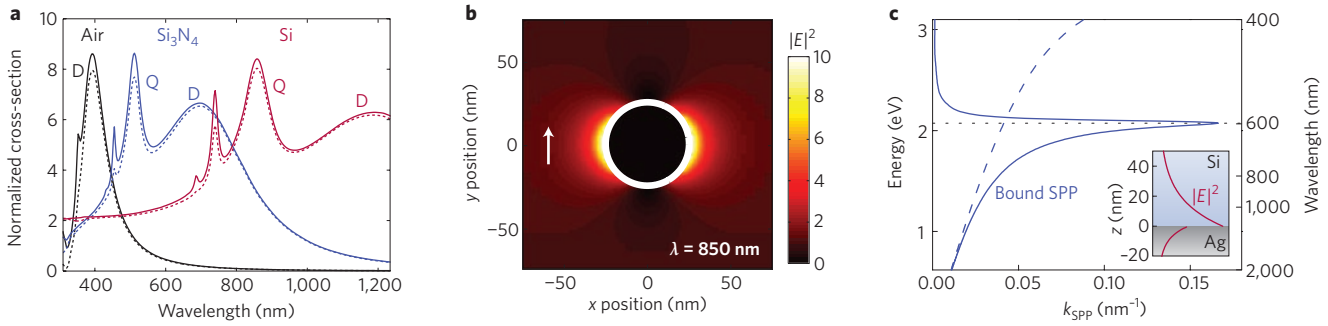

Figure 4 | Characteristics of surface plasmons. a, Metal nanoparticles scatter light over a broad spectral range that can be tuned by the surrounding dielectric. The plots show the scattering cross-section spectrum for a 100-nm-diameter Ag particle embedded in three different dielectrics (air, Si_3N_4 and Si). Dipole (D) and quadrupole (Q) modes are indicated. The cross-section is normalized to the geometrical cross-section of the particle. **b**, Metal nanoparticles show an intense near-field close to the surface. Intensity enhancement around a 25-nm-diameter Au particle embedded in a medium with index $n = 1.5$ (plasmon resonance peak at 500 nm). Light with a wavelength $\lambda = 850$ nm is incident with a polarization indicated by the vertical arrow. The magnitude of the enhanced electric-field intensity E is indicated by the colour scale. **c**, SPPs are bound waves at the interface between a semiconductor and a dielectric. This dispersion diagram, plotting the relationship between frequency and wavevector ($2\pi/\lambda$) for SPPs on a Ag/Si interface. The 'bound' SPP mode occurs at energies below the surface plasmon resonance energy of 2.07 eV (600 nm). The dispersion of light in Si is indicated by the dashed line. The inset shows a schematic of the SPP mode profile along the Si/Ag interface, at a free-space wavelength of 785 nm.

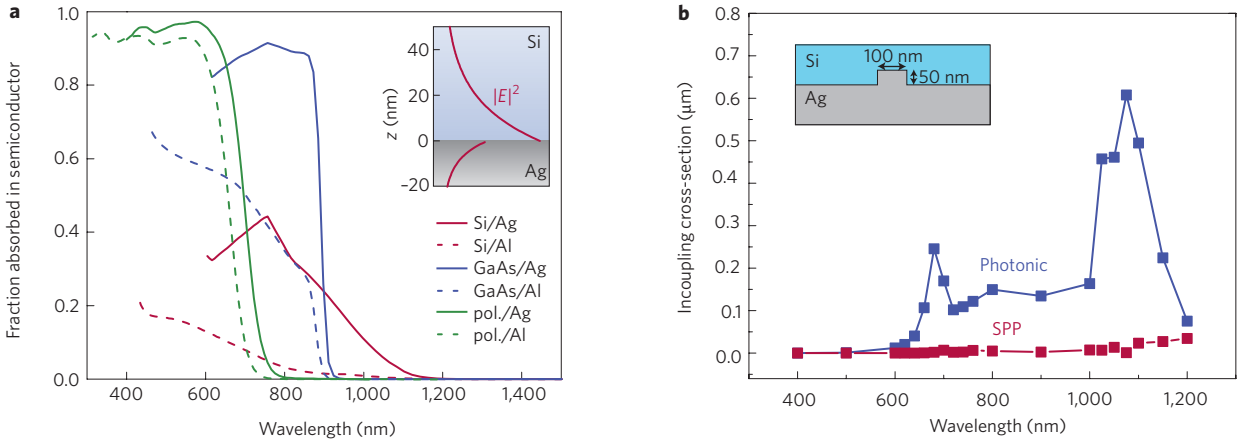

Figure 5 | Light scattering into SPP and photonic modes in thin semiconductor films. a, Fraction of light absorbed into the semiconductor for SPPs propagating along interfaces between semi-infinite layers of GaAs, Si and an organic semiconductor film made of a PF10TBT:[C60]PCBM polymer blend (termed 'pol.' in the legend), in contact with either Ag or Al. Graphs are plotted for wavelength down to the surface plasmon resonance. The inset shows the SPP field intensity near the interface. **b**, Two-dimensional calculation of the incoupling cross-section for SPP and photonic modes as a function of wavelength for a 200-nm-thick Si slab on an optically thick Ag substrate with a 100-nm-wide, 50-nm-tall Ag ridge, as shown in the inset. Figure reproduced with permission: **b**, © 2008 ACS.

Light trapping using SPPs. In a third plasmonic light-trapping geometry, light is converted into SPPs, which are electromagnetic waves that travel along the interface between a metal back contact and the semiconductor absorber layer (see Fig. 4c)[60]. Near the plasmon resonance frequency, the evanescent electromagnetic SPP fields are confined near the interface at dimensions much smaller than the wavelength. SPPs excited at the metal/semiconductor interface can efficiently trap and guide light in the semiconductor layer. In this geometry the incident solar flux is effectively turned by 90°, and light is absorbed along the lateral direction of the solar cell, which has dimensions that are orders of magnitude larger than the optical absorption length. As metal contacts are a standard element in the solar-cell design, this plasmonic coupling concept can be integrated in a natural way.

At frequencies near the plasmon resonance frequency (typically in the 350–700 nm spectral range, depending on metal and dielectric) SPPs suffer from relatively high losses. Further into the infrared, however, propagation lengths are substantial. For example, for a semi-infinite Ag/SiO_2 geometry, SPP propagation lengths range from 10 to 100 μm in the 800–1,500 nm spectral range. By using a thin-film metal geometry the plasmon dispersion can be further engineered[61–64]. Increased propagation length comes at the expense of reduced optical confinement and optimum metal-film design thus depends on the desired solar-cell geometry. Detailed accounts of plasmon dispersion and loss in metal–dielectric geometries are found in refs 61–64.

The SPP coupling mechanism is beneficial for efficient light absorption if absorption of the SPP in the semiconductor is stronger than in the metal. This is illustrated in Fig. 5a, which shows a calculation of the fraction of light that is absorbed in a silicon or GaAs film in contact with either Ag or Al. The inset shows the mode-field distribution at the Si/Ag interface at a wavelength of 850 nm. As can be seen, for SPPs at a GaAs/Ag interface the semiconductor absorption fraction is high in the spectral range from the GaAs/Ag SPP resonance (600 nm) to the bandgap of GaAs (870 nm). For a Si/Ag interface, with smaller optical absorption in Si owing to the indirect bandgap, plasmon losses dominate over the entire spectral range, although absorption in the 700–1,150 nm spectral range is

still higher than single-pass absorption through a 1-μm-thick Si film. In this case, it is more beneficial to use a geometry in which a thin metal film is embedded in the semiconductor, as in this case plasmon absorption is much smaller owing to the smaller mode overlap with the metal[63,64]. Figure 5a also shows a calculation of the absorption of an organic semiconductor (PF10TBT:[C60]PCBM) (ref. 65) in contact with Ag or Al. Optical constants for the polymer are taken from ref. 65. Here the absorption efficiency is high over the entire spectral range below 650 nm because the organic semiconductor has high absorption, and the low dielectric constant of the organic material causes a small overlap of the modal field with the metal and thus lower ohmic losses.

Owing to the momentum mismatch between the incident light and the in-plane SPPs (see Fig. 4c) a light-incoupling structure must be integrated in the metal/dielectric interface. Figure 5b plots the results of full-field electrodynamics simulations (taking into account in- and outcoupling) of the scattering from an incident plane wave into SPPs by a ridge fabricated in the Ag/Si interface[66]. The Si layer is 200 nm thick and the Ag ridge 50 nm tall. The simulations show that light is coupled into an SPP mode as well as a photonic mode that propagates inside the Si waveguide, and that the strength of coupling to each mode can be controlled by the height of the scattering object[66]. The photonic modes are particularly interesting as they suffer from only very small losses in the metal. The fraction of light coupled into both modes increases with increasing wavelength. This is mainly because at shorter wavelengths the incoming light beam is directly absorbed in the Si layer. The data demonstrate that light with $\lambda > 800$ nm, which would not be well absorbed by normal incidence on the Si layer (see Fig. 1a), can now be efficiently absorbed by conversion into the in-plane SPP and photonic modes. Although this example shows coupling from a single, isolated ridge, the shape, height and interparticle arrangements of incoupling structures can all be optimized for preferential coupling to particular modes. In the ultimate, ultrathin Si solar cell (thickness <100 nm), no photonic modes exist and all scattered light is converted into SPPs. Further enhancements are expected for three-dimensional scattering structures integrated in the back contact, and more research is required to investigate this. Most recently, we have reported experiments on amorphous Si thin-film solar cells deposited on a textured metal back reflector, which show a 26% enhancement in short-circuit current, with the primary photocurrent enhancement in the near-infrared[67].

In relation to the plasmonic coupling effect, a similar conversion mechanism into surface polariton waves has recently been demonstrated using lossy dielectrics rather than metals[68]. Here too, light is efficiently coupled into a two-dimensional wave that can then be absorbed in a semiconductor layer. Several other reports on the integration of SPP geometries with thin-film solar-cell geometries are now appearing, including organic solar cells[69–71].

The data in Fig. 5b were calculated for light under normal incidence, with a polarization perpendicular to the ridge. The next challenge is to engineer coupling structures that depend weakly on frequency, polarization and angle of incidence. A two-dimensional mesh structure with features much smaller than the wavelength may serve such a purpose.

It is clear that with these scattering structures made on the rear side of the cell, the concepts of plasmonic scattering, concentration and coupling from this section and the previous two sections become closely integrated. Indeed, any solar cell with a non-planar metal back contact will have geometric scattering and higher local fields as well as scattering into photonic and plasmonic modes, and all these effects must be carefully engineered. We note that there is at present considerable activity on thin-film solar cells with textured metal back reflectors for light trapping[72–77].

Advantages of reduced semiconductor absorber layer thickness. The plasmonic light-trapping concepts described in the previous sections lead to new solar-cell designs with smaller semiconductor thicknesses and thus lower material costs. This has important technical and strategic consequences as photovoltaics scales-up in manufacturing capacity from its present level of ~8 GW in 2009 to >50 GW by 2020, and eventually to the terawatt scale. For this to happen, the materials used in solar cells must be sufficiently abundant in the Earth's crust and amenable to the formation of efficient photovoltaic devices. For single-junction devices, Si has proved to be a near-ideal photovoltaic material. It is abundant, with a nearly optimal bandgap, excellent junction formation characteristics, high minority carrier diffusion length and effective methods for surface passivation to reduce unwanted carrier recombination. Its only shortcoming — low spectral absorption of the terrestrial solar spectrum — means that it requires cell thicknesses of over 100 μm, which gives rise to a relatively high material cost per output power. Plasmonic light trapping makes it possible to design crystalline Si thin-film cells with spectral quantum efficiency approaching that seen in thick cells, even for absorber layers a few micrometres in thickness.

Materials resources are a significant limitation for large-scale production of two of the most common thin-film solar-cell materials: CdTe and $CuInSe_2$. Manufacturing costs for these cells have fallen, and solar-cell production using these semiconductors is expanding rapidly. Table 1 lists the (projected) annual solar-cell production per year, as well as the materials feedstock required for the production of the corresponding solar-cell volume using Si, CdTe or $CuInSe_2$. As can be seen, the materials feedstock required in 2020 exceeds the present annual world production of Te and In, and in the case of In is even close to the total reserve base. If it were possible to reduce the cell thickness for such compound semiconductor cells by 10–100 times as a result of plasmon-enhanced light absorption, this could considerably extend the reach of these compound semiconductor thin-film solar cells towards the terawatt scale. Earth-abundance considerations will also influence plasmonic cell designs at large-scale production: although Ag and Au have been the metals of choice in most plasmonic designs and experiments, they are relatively scarce materials, so scalable designs will need to focus on abundant metals such as Al and Cu.

Reducing the active-layer thickness by plasmonic light trapping not only reduces costs but also improves the electrical characteristics of the solar cell[78]. First of all, reducing the cell thickness reduces the dark current (I_{dark}), causing the open-circuit voltage V_{oc} to increase, as $V_{oc} = (k_B T/q) \ln(I_{photo}/I_{dark} + 1)$, where k_B is the Boltzmann constant, T is temperature, q is the charge and I_{photo} is the photocurrent. Consequently, the cell efficiency rises in logarithmic proportion to the decrease in thickness, and is ultimately

Table 1 | Photovoltaic resource requirements: materials by production and reserve.

Year	Annual solar-cell production*	Material		
		Si (c-Si)	Te (CdTe)	In ($CuInSe_2$)
2000	0.3 GW_p	4	0.03	0.03
2005	1.5 GW_p	15	0.15	0.15
2020	50 GW_p	150	5	5
World production (1,000 tonnes per year)		1,000	0.3	0.5
Reserve base (1,000 tonnes)		Abundant	47	6

*W_p = peak output power under full solar illumination.
The annual solar-cell production and the required materials feedstock are indicated, assuming cells are made of Si, CdTe or $CuInSe_2$. The assumed material use for Si is 13 g W_p^{-1} in 2000, 10 g W_p^{-1} in 2005, 3 g W_p^{-1} in 2020 (projected); it is 0.1 g W_p^{-1} for Te and In. The two bottom rows indicate the world reserve base data for Si, Te and In (that is, resources that are economic at present or marginally economic and some that are at present subeconomic).
Sources: refs 93, 94 and G. Willeke (Fraunhofer Institute for Solar Energy Systems), personal communication.

limited by surface recombination. Second, in a thin-film geometry, carrier recombination is reduced as carriers need to travel only a small distance before being collected at the junction. This leads to a higher photocurrent. Greatly reducing the semiconductor layer thickness allows the use of semiconductor materials with low minority carrier diffusion lengths, such as polycrystalline semiconductors, quantum-dot layers or organic semiconductors. Also, this could render useful abundant and potentially inexpensive semiconductors with significant impurity and defect densities, such as Cu_2O, Zn_3P_2 or SiC, for which the state of electronic materials development is not as advanced as it is for Si.

Other new plasmonic solar-cell designs

The previous section has focused on the use of plasmonic scattering and coupling concepts to improve the efficiency of single-junction planar thin-film solar cells, but many other cell designs can benefit from the increased light confinement and scattering from metal nanostructures. First of all, plasmonic 'tandem' geometries may be made, in which semiconductors with different bandgaps are stacked on top of each other, separated by a metal contact layer with a plasmonic nanostructure that couples different spectral bands in the solar spectrum into the corresponding semiconductor layer (see Fig. 6a)[79]. Coupling sunlight into SPPs could also solve the problem of light absorption in quantum-dot solar cells (see Fig. 6b). Although such cells offer potentially large benefits because of the flexibility in engineering the semiconductor bandgap by particle size, effective light absorption requires thick quantum-dot layers, through which carrier transport is problematic. As we have recently demonstrated[80], a 20-nm-thick layer of CdSe semiconductor quantum dots deposited on a Ag film can absorb light confined into SPPs within a decay length of 1.2 μm at an incident photon energy above the CdSe quantum-dot bandgap at 2.3 eV. The reverse geometry, in which quantum dots are electrically excited to generate plasmons, has also recently been demonstrated[81]. We note that the plasmon light-trapping concepts described in the previous section rely on scattering using localized modes, and are thus relatively insensitive to angle of incidence[66,82]. This is an advantage for solar-cell designs made for areas where incident sunlight is mostly diffuse rather than direct.

In a recent example of nanoscale plasmonic solar-cell engineering, an organic photovoltaic light absorber was integrated in the gap between the arms of plasmonic antennas arranged in arrays (see Fig. 6c)[83]. Other examples of nanoscale antennas are coaxial holes fabricated in a metal film, which show localized plasmonic modes owing to Fabry–Perot resonances (see Fig. 6d)[84–86]. Such nanostructures, with field enhancements up to a factor of about 50, could be used in entirely new solar-cell designs, in which an inexpensive semiconductor with low minority carrier lifetime is embedded inside the plasmonic cavity. Similarly, quantum-dot solar cells based on multiple-exciton generation[87], or cells with solar upconverters or downconverters based on multiphoton absorption effects, could benefit from such plasmonic field concentration. In general, field concentration in plasmonic nanostructures is likely to be useful in any type of solar cell where light concentration is

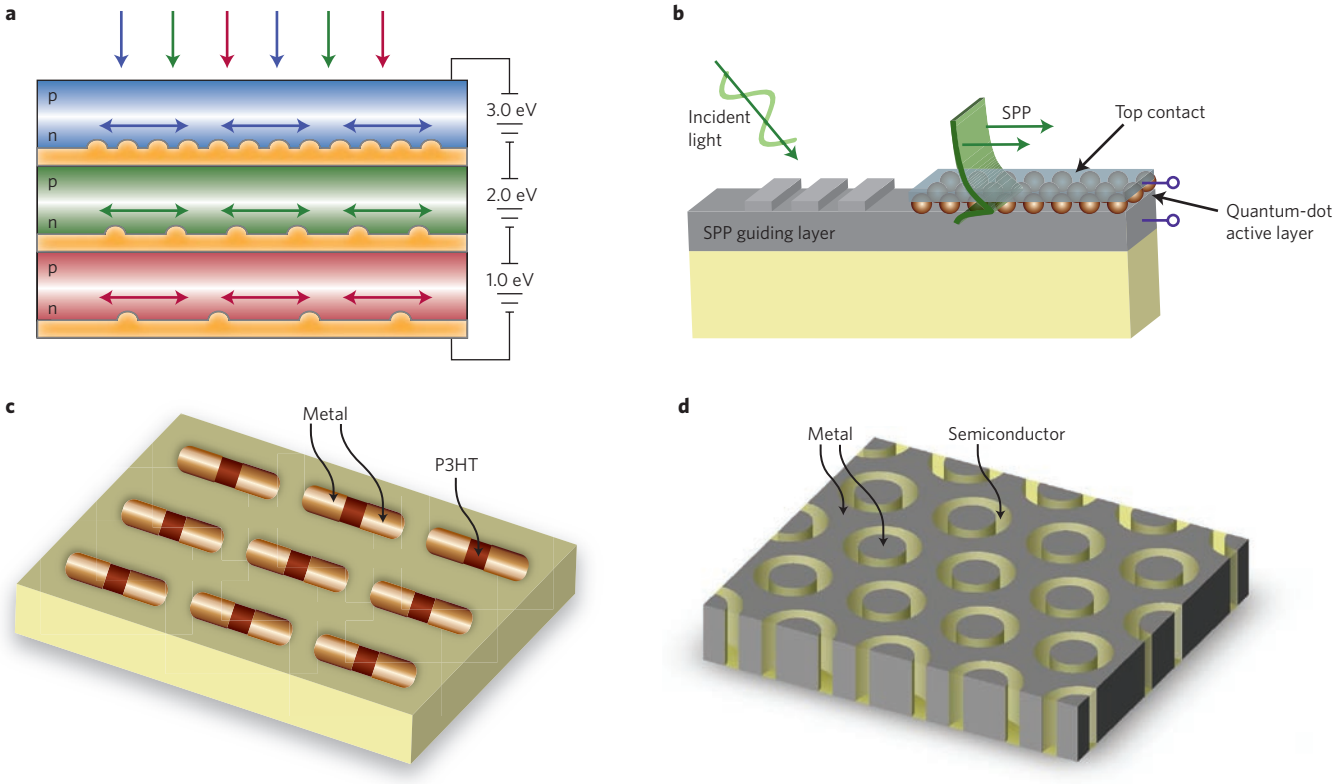

Figure 6 | New plasmonic solar-cell designs. a, Plasmonic tandem solar-cell geometry. Semiconductors with different bandgaps are stacked on top of each other, separated by a metal contact layer with a plasmonic nanostructure that couples different spectral bands of the solar spectrum into the corresponding semiconductor layer. **b**, Plasmonic quantum-dot solar cell designed for enhanced photoabsorption in ultrathin quantum-dot layers mediated by coupling to SPP modes propagating in the plane of the interface between Ag and the quantum-dot layer. Semiconductor quantum dots are embedded in a metal/insulator/metal SPP waveguide. **c**, Optical antenna array made from an axial heterostructure of metal and poly(3-hexylthiophene) (P3HT). Light is concentrated in the nanoscale gap between the two antenna arms, and photocurrent is generated in the P3HT semiconductor[83]. **d**, Array of coaxial holes in a metal film that support localized Fabry–Perot plasmon modes. The coaxial holes are filled with an inexpensive semiconductor with low minority carrier lifetime, and carriers are collected by the metal on the inner and outer sides of the coaxial structure. Field enhancements up to a factor of about 50 are possible and may serve to enhance nonlinear photovoltaic conversion effects[85].

beneficial, such as a high-efficiency multijunction solar cells[88,89]. More details on plasmon light concentration are found in another review in this issue[90].

Large-area fabrication of plasmonic solar-cell structures

The plasmonic coupling effects described in this review all require integration of dense arrays of metal nanostructures with control over dimension tolerances at the nanometre scale. Although systematic laboratory experiments can be performed using cleanroom techniques such as electron-beam lithography or focused ion-beam milling, true application in large-area photovoltaic module production requires inexpensive and scalable techniques for fabricating metal nanopatterns in a controlled way. Several research groups have studied these techniques and have shown their feasibility.

The simplest way to form metal nanoparticles on a substrate is by thermal evaporation of a thin (10–20 nm) metal film, which is then heated at a moderate temperature (200–300 °C), to cause agglomeration by surface tension of the metal film into a random array of nanoparticles. As has been shown[35,42], this leads to the formation of random arrays of Ag nanoparticles with a diameter (100–150 nm) and hemispherical shape that is well suited for light trapping[38]. More control over the Ag nanoparticle size, aspect ratio and density can be achieved using deposition through a porous alumina template, as was demonstrated for example in ref. 37. Here, the nanoparticle shape was further tuned by thermal annealing at 200 °C, leading to hemispherical particles as well. More recently, substrate conformal imprint lithography[91] has been developed, in which a sol–gel mask is defined by soft lithography using a rubber stamp, followed by Ag evaporation and lift-off. This process leads to <0.1 nm control over particle pitch. Examples of nanopatterns fabricated using these three techniques are shown in Fig. 7a–c. Figure 7d shows a photograph of a 6-inch-diameter Si wafer structured using soft lithography with a regular array of metal nanoparticles.

Integration of metallic nanostructures on the surface of a solar cell can also reduce the cell surface sheet resistance, which leads to greater output power as well[37]. Indeed, in an optimized plasmonic solar-cell design, the metal nanostructures will be integrated with the metal-finger structure that conventionally collects current from the cell. In further advanced designs, a percolating metal nanostructure may itself be used as a means to collect the photocurrent. An inverse structure using metal hole arrays for light concentration and collection has also been demonstrated[92]. Using nanoscale metal contacts could potentially reduce the optical reflection loss that typically results from the coverage of a solar cell by macroscopic metal fingers.

Summary and outlook

The ability to construct optically thick but physically very thin photovoltaic absorbers could revolutionize high-efficiency photovoltaic device designs. This becomes possible by using light trapping through the resonant scattering and concentration of light in arrays of metal nanoparticles, or by coupling light into surface plasmon polaritons and photonic modes that propagate in the plane of the semiconductor layer. In this way extremely thin photovoltaic absorber layers (tens to hundreds of nanometres thick) may absorb the full solar spectrum.

Because of the small required thickness, relatively impure and defective semiconductor absorbers (for example polycrystalline films of Si, Cu_2O, Zn_3P_2 or SiC) may be used, without suffering from volume recombination losses. The use of thin absorber layers also avoids some of the problems of materials scarcity for compound semiconductors.

Guiding and concentration of light using plasmonic geometries allows entirely new solar-cell designs in which light is fully absorbed in a single quantum well, or in a single layer of quantum dots or molecular chromophores. This would also open up new approaches to carrier collection from quantum-well and quantum-dot solar cells that do not rely on inter-well or inter-dot carrier transfer before photocarrier collection at the device contacts. The extreme confinement of light that can be achieved using plasmonic nanostructures can also enhance nonlinear effects such as up- and down-conversion or multiple carrier generation in nanoscale solar-cell geometries.

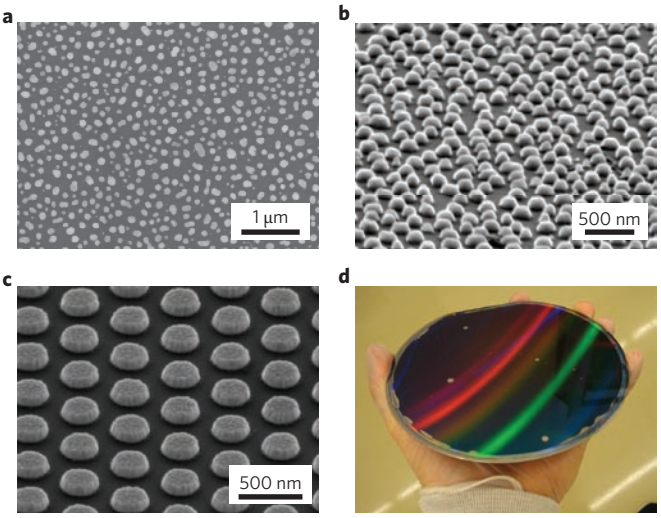

Figure 7 | Large-area metal nanopatterns for plasmonic solar cells. **a**–**c**, Scanning electron micrographs of arrays of Ag nanoparticles. **a**, A 14-nm-thick Ag film was deposited onto a thermally oxidized Si wafer (SiO_2 thickness 10 nm) by thermal evaporation and annealed at 200 °C in a N_2 ambient atmosphere for 60 minutes in forming gas. Silver nanoparticles form by surface-tension-induced agglomeration. The average particle diameter is 135 nm, and surface coverage is 26%. **b**, Silver nanoparticles evaporated through a porous alumina template, annealed at 200 °C. The average particle diameter is 135 nm. **c**, Hexagonal array of Ag nanoparticles deposited using substrate-conformal imprint lithography using the SCIL technique. The particle diameter is 300 nm. From M. A. Verschuuren, P. Gerlach, A. Polman and H. A. van Sprang, manuscript in preparation. **d**, Wafer-scale metal nanopatterns made using the SCIL technique. From M. A. Verschuuren, Y. Ni, M. Megens, H. A. van Sprang and A. Polman, manuscript in preparation. Figures reproduced with permission: **a**, © 2007 AIP; **b**, © 2008 AIP.

Corrected online 1 September 2010

References

1. Green, M. A. *Solar Cells: Operating Principles, Technology and System Applications* (Univ. New South Wales, 1998).
2. Yablonovitch, E. & Cody, G. D. Intensity enhancement in textured optical sheets for solar cells. *IEEE Trans. Electr. Dev.* **29,** 300–305 (1982).
3. Deckman, H. W., Roxlo, C. B. & Yablonovitch, E. Maximum statistical increase of optical absorption in textured semiconductor films. *Opt. Lett.* **8,** 491–493 (1983).
4. Polman, A. Plasmonics applied. *Science* **322,** 868 (2008).
5. Andrew, P. & Barnes, W. L. Energy transfer across a metal film mediated by surface plasmon polaritons. *Science* **306,** 1002–1005 (2004).
6. Mertens, H., Biteen, J. S., Atwater, H. A. & Polman, A. Polarization-selective plasmon-enhanced Si quantum dot luminescence. *Nano Lett.* **6,** 2622–2625 (2006).
7. Kühn, S., Hakanson, U., Rogobete, L. & Sandoghdar, V. Enhancement of single molecule fluorescence using a gold nanoparticle as an optical nano-antenna. *Phys. Rev. Lett.* **97,** 017402 (2006).
8. Stockman, M. I. Nanofocusing of optical energy in tapered plasmonic waveguides. *Phys. Rev. Lett.* **93,** 137404 (2004).
9. Verhagen, E., Spasenović, M., Polman, A. & Kuipers, L. Nanowire plasmon excitation by adiabatic mode transformation. *Phys. Rev. Lett.* **102,** 203904 (2008).
10. Prodan, E., Radloff, C., Halas, N. J. & Nordlander, P. A hybridization model for the plasmon response of complex nanostructures. *Science* **302,** 419–422 (2003).
11. Quinten, M., Leitner, A., Krenn, J. R. & Aussenegg, F. R. Electromagnetic energy transport via linear chains of silver nanoparticles. *Opt. Lett.* **23,** 1331–1333 (1998).

12. Maier, S. A. *et al.* Local detection of electromagnetic energy transport below the diffraction limit in metal nanoparticle plasmon waveguides. *Nature Mater.* **2,** 229–232 (2003).
13. Koenderink, A. F. & Polman, A. Complex response and polariton-like dispersion splitting in periodic metal nanoparticle chains. *Phys. Rev. B* **74,** 033402 (2006).
14. Zia, R., Selker, M. D., Catrysse, P. B. & Brongersma, M. L. Geometries and materials for subwavelength surface plasmon modes. *J. Opt. Soc. Am. A* **21,** 2442–2446 (2004).
15. Mühlschlegel, P., Eisler, H. J., Martin, O. J. F., Hecht, B. & Pohl, D. W. Resonant optical antennas. *Science* **308**, 1607–1609 (2005).
16. Ditlbacher, H., Krenn, J. R., Schider, G., Leitner, A. & Aussenegg, F. R. Two-dimensional optics with surface plasmon polaritons. *Appl. Phys. Lett.* **81,** 1762–1764 (2002).
17. Bozhevolnyi, S. I., Volkov, V. S., Devaux, E., Laluet, J. Y. & Ebbesen, T. W. Channel plasmon subwavelength waveguide components including interferometers and ring resonators. *Nature* **440,** 508–511 (2006).
18. Krasavin, A. V. & Zheludev, N. I. Active plasmonics: Controlling signals in Au/Ga waveguide using nanoscale structural transformations. *Appl. Phys. Lett.* **84,** 1416–1418 (2004).
19. Colombelli, R. *et al.* Quantum cascade surface-emitting photonic crystal laser. *Science* **302,** 1374–1377 (2003).
20. Hill, M. T. *et al.* Lasing in metallic-coated nanocavities. *Nature Photon.* **1,** 589–594 (2007).
21. Oulton, R. F. *et al.* Plasmon lasers at deep subwavelength scale. *Nature* **461,** 629–632 (2009).
22. Okamoto, K. *et al.* Surface-plasmon-enhanced light emitters based on InGaN quantum wells. *Nature Mater.* **3,** 601–605 (2004).
23. Pendry, J. B. Negative refraction makes a perfect lens. *Phys. Rev. Lett.* **85,** 3966–3968 (2000).
24. Shelby, R. A., Smith, D. R. & Schultz, S. Experimental verification of a negative index of refraction. *Science* **292,** 77–79 (2001).
25. Linden, S. *et al.* Magnetic response of metamaterials at 100 terahertz. *Science* **306,** 1351–1353 (2004).
26. Fang, N., Lee, H., Sun, C. & Zhang, X. Sub-diffraction-limited optical imaging with a silver superlens. *Science* **308,** 534–537 (2005).
27. Kreibig, U. & Vollmer, M. *Optical Properties of Metal Clusters* (Springer, 1995).
28. Bohren, C. F. & Huffman, D. R. *Absorption and Scattering of Light by Small Particles* (Wiley, 2008).
29. Mertz, J. Radiative absorption, fluorescence, and scattering of a classical dipole near a lossless interface: a unified description. *J. Opt. Soc. Am. B* **17,** 1906–1913 (2000).
30. Stuart, H. R. & Hall, D. G. Absorption enhancement in silicon-on-insulator waveguides using metal island films. *Appl. Phys. Lett.* **69,** 2327–2329 (1996).
31. Stuart, H. R. & Hall, D. G. Island size effects in nanoparticle-enhanced photodetectors. *Appl. Phys. Lett.* **73,** 3815–3817 (1998).
32. Schaadt, D. M., Feng, B. & Yu, E. T. Enhanced semiconductor optical absorption via surface plasmon excitation in metal nanoparticles. *Appl. Phys. Lett.* **86,** 063106 (2005).
33. Derkacs, D., Lim, S. H., Matheu, P., Mar, W. & Yu, E. T. Improved performance of amorphous silicon solar cells via scattering from surface plasmon polaritons in nearby metallic nanoparticles. *Appl. Phys. Lett.* **89,** 093103 (2006).
34. Matheu, P., Lim, S. H., Derkacs, D., McPheeters, C. & Yu, E. T. Metal and dielectric nanoparticle scattering for improved optical absorption in photovoltaic devices. *Appl. Phys. Lett.* **93,** 113108 (2008).
35. Pillai, S., Catchpole, K. R., Trupke, T. & Green, M. A. Surface plasmon enhanced silicon solar cells. *J. Appl. Phys.* **101,** 093105 (2007).
36. Derkacs, D. *et al.* Nanoparticle-induced light scattering for improved performance of quantum-well solar cells. *Appl. Phys. Lett.* **93,** 091107 (2008).
37. Nakayama, K., Tanabe, K. & Atwater, H. A. Plasmonic nanoparticle enhanced light absorption in GaAs solar cells. *Appl. Phys. Lett.* **93,** 121904 (2008).
38. Catchpole, K. R. & Polman, A. Design principles for particle plasmon enhanced solar cells. *Appl. Phys. Lett.* **93,** 191113 (2008).
39. Catchpole, K. R. & Polman, A. Plasmonic solar cells. *Opt. Express* **16,** 21793–21800 (2008).
40. Xu, G., Tazawa, M., Jin, P., Nakao, S. & Yoshimura, K. Wavelength tuning of surface plasmon resonance using dielectric layers on silver island films. *Appl. Phys. Lett.* **82,** 3811–3813 (2003).
41. Mertens, H., Verhoeven, J., Polman, A. & Tichelaar, F. D. Infrared surface plasmons in two-dimensional silver nanopartice arrays in silicon. *Appl. Phys. Lett.* **85,** 1317–1319 (2004).
42. Beck, F. J., Polman, A. & Catchpole, K. R. Tunable light trapping for solar cells using localized surface plasmons. *J. Appl. Phys.* **105,** 114310 (2009).
43. Lim, S. H., Mar, W., Matheu, P., Derkacs, D. & Yu, E. T. Photocurrent spectroscopy of optical absorption enhancement in silicon photodiodes via scattering from surface plasmon polaritons in gold nanoparticles. *J. Appl. Phys.* **101,** 104309 (2007).
44. Beck, F. J., Mokkapati, S., Polman, A. & Catchpole, K. R. Asymmetry in light-trapping by plasmonic nanoparticle arrays located on the front or on the rear of solar cells. *Appl. Phys. Lett.* (in the press).
45. Pala, R. A., White, J., Barnard, E., Liu, J. & Brongersma, M. L. Design of plasmonic thin-film solar cells with broadband absorption enhancements. *Adv. Mater.* **21,** 3504–3509 (2009).
46. Mokkapati, S., Beck, F. J., Polman, A. & Catchpole, K. R. Designing periodic arrays of metal nanoparticles for light trapping applications in solar cells. *Appl. Phys. Lett.* **95,** 53115 (2009).
47. Stuart, H. R. & Hall, D. G. Thermodynamic limit to light trapping in thin planar structures. *J. Opt. Soc. Am. A* **14,** 3001–3008 (1997).
48. Stuart, H. R. & Hall, D. G. Enhanced dipole–dipole interaction between elementary radiators near a surface. *Phys. Rev. Lett.* **80,** 5663–5668 (1998).
49. Catchpole, K. R. & Pillai, S. Absorption enhancement due to scattering by dipoles into silicon waveguides. *J. Appl. Phys.* **100,** 044504 (2006).
50. Rand, B. P., Peumans, P. & Forrest, S. R. Long-range absorption enhancement in organic tandem thin-film solar cells containing silver nanoclusters. *J. Appl. Phys.* **96,** 7519–7526 (2004).
51. Kim, S. S., Na, S.-I., Jo, J., Kim, D. Y. & Nah, Y.-C. Plasmon enhanced performance of organic solar cells using electrodeposited Ag nanoparticles. *Appl. Phys. Lett.* **93,** 073307 (2008).
52. Morfa, A. J., Rowlen, K. L., Reilly, T. H., Romero, M. J. & Van de Lagemaat, J. Plasmon-enhanced solar energy conversion in organic bulk heterojunction photovoltaics. *Appl. Phys. Lett.* **92,** 013504 (2008).
53. Lindquist, N. C., Luhman, W. A., Oh, S. H. & Holmes, R. J. Plasmonic nanocavity arrays for enhanced efficiency in organic photovoltaic cells. *Appl. Phys. Lett.* **93,** 123308 (2008).
54. Kume, T., Hayashi, S., Ohkuma, H., Yamamoto, K. Enhancement of photoelectric conversion efficiency in copper phthalocyanine solar cell: white light excitation of surface plasmon polaritons. *Jpn. J. Appl. Phys.* **34,** 6448–6451 (1995).
55. Westphalen, M., Kreibig, U., Rostalski, J., Lüth, H. & Meissner, D. Metal cluster enhanced organic solar cells. *Sol. Energy Mater. Sol. C.* **61,** 97–105 (2000).
56. Hägglund, C., Zäch, M. & Kasemo, B. Enhanced charge carrier generation in dye sensitized solar cells by nanoparticle plasmons. *Appl. Phys. Lett.* **92,** 013113 (2008).
57. Konda, R. B. *et al.* Surface plasmon excitation via Au nanoparticles in n-CdSe/p-Si heterojunction diodes. *Appl. Phys. Lett.* **91,** 191111 (2007).
58. Hägglund, C., Zäch, M., Petersson, G. & Kasemo, B. Electromagnetic coupling of light into a silicon solar cell by nanodisk plasmons. *Appl. Phys. Lett.* **92,** 053110 (2008).
59. Kirkengena, M., Bergli, J. & Galperin, Y. M. Direct generation of charge carriers in c-Si solar cells due to embedded nanoparticles. *J. Appl. Phys.* **102,** 093713 (2007).
60. Raether, H. *Surface Plasmons on Smooth and Rough Surfaces and on Gratings*. (Springer Tracts in Modern Physics III, Springer, 1988).
61. Berini, P. Plasmon–polariton waves guided by thin lossy metal films of finite width: bound modes of symmetric structures. *Phys. Rev. B* **61,** 10484–10503 (2000).
62. Berini, P. Plasmon–polariton waves guided by thin lossy metal films of finite width: bound modes of asymmetric structures. *Phys. Rev. B* **63,** 125417 (2001).
63. Dionne, J. A., Sweatlock, L., Atwater, H. A. & Polman, A. Planar plasmon metal waveguides: frequency-dependent dispersion, propagation, localization, and loss beyond the free electron model. *Phys. Rev. B* **72,** 075405 (2005).
64. Dionne, J. A., Sweatlock, L., Atwater, H. A. & Polman, A. Plasmon slot waveguides: towards chip-scale propagation with subwavelength-scale localization. *Phys. Rev. B* **73,** 035407 (2006).
65. Slooff, L. H. *et al.* Determining the internal quantum efficiency of highly efficient polymer solar cells through optical modeling. *Appl. Phys. Lett.* **90,** 143506 (2007).
66. Ferry, V. E., Sweatlock, L. A., Pacifici, D. & Atwater, H. A. Plasmonic nanostructure design for efficient light coupling into solar cells. *Nano Lett.* **8,** 4391–4397 (2008).
67. Ferry, V. *et al.* Improved red-response in thin film a-Si:H solar cells with nanostructured plasmonic back reflectors. *Appl. Phys. Lett.* **95,** 183503 (2009).
68. Giannini, V., Zhang, Y., Forcales, M. & Gómez Rivas, J. Long-range surface plasmon polaritons in ultra-thin films of silicon. *Opt. Express* **16,** 19674–19685 (2008).
69. Mapel, J. K., Singh, M., Baldo, M. A. & Celebi, K. Plasmonic excitation of organic double heterostructure solar cells. *Appl. Phys. Lett.* **90,** 121102 (2007).
70. Tvingstedt, K., Persson, N. K., Ingan, O., Rahachou, A. & Zozoulenko, I. V. Surface plasmon increase absorption in polymer photovoltaic cells. *Appl. Phys. Lett.* **91,** 113514 (2007).
71. Heidel, T. D., Mapel, J. K., Singh, M., Celebi, K. & Baldo, M. A. Surface plasmon polariton mediated energy transfer in organic photovoltaic devices. *Appl. Phys. Lett.* **91,** 093506 (2007).
72. Haug, F. J., Söderström, T., Cubero, O., Terrazzoni-Daudrix, V. & Ballif, C. Plasmonic absorption in textured silver back reflectors of thin film solar cells. *J. Appl. Phys.* **104,** 064509 (2008).

73. Tvingstedt, K., Person, N. K., Inganäs, O., Rahachou, A. & Zozoulenko, I. V. Surface plasmon increase absorption in polymer photovoltaic cells. *Appl. Phys. Lett.* **91,** 113514 (2007).
74. Franken, R. H. *et al.* Understanding light trapping by light-scattering textured back electrodes in thin-film n–i–p silicon solar cells. *J. Appl. Phys.* **102,** 014503 (2007).
75. Schropp, R. E. I. *et al.* Nanostructured thin films for multibandgap silicon triple junction solar cells. *Sol. Energy Mater. Sol. C.* **93,** 1129–1133 (2009).
76. Rockstuhl, C., Fahr, S. & Lederer, F. Absorption enhancement in solar cells by localized plasmon polaritons. *J. Appl. Phys.* **104,** 123102 (2008).
77. Keevers, M. J., Young, T. L., Schubert, U. & Green, M. A. 10% efficient CSG minimodules. *Proc. 22nd Eur. Photovoltaic Solar Energy Conf.* Milan, Italy, 3–7 September 2007.
78. Green, M. A., Zhao, J., Wang, A. & Wenham, S. R. Very high efficiency silicon solar cells: science and technology. *IEEE Trans. Electr. Dev.* **46,** 1940–1947 (1999).
79. Fahr, S., Rockstuhl, C. & Lederer, F. Metallic nanoparticles as intermediate reflectors in tandem solar cells. *Appl. Phys. Lett.* **95,** 121105 (2009).
80. Pacifici, D., Lezec, H. & Atwater, H. A. All-optical modulation by plasmonic excitation of CdSe quantum dots. *Nature Photon.* **1,** 402–406 (2007).
81. Walters, R. J., van Loon, R. V. A., Brunets, I., Schmitz, J. & Polman, A. A silicon-based electrical source of surface plasmon polaritons. *Nature Mater.* **9,** 21–25 (2010).
82. Verhagen, E., Kuipers, L. & Polman, A. Field enhancement in metallic subwavelength aperture arrays probed by erbium upconversion luminescence. *Opt. Express* **17,** 14586–14597 (2009).
83. O'Carroll, D., Hofmann, C. E. & Atwater, H. A. Conjugated polymer/metal nanowire heterostructure plasmonic antennas. *Adv. Mater.* doi:10.1002/adma.200902024 (2009).
84. Labeke, D. V., Gerard, D., Guizal, B., Baida, F. I. & Li, L. An angle-independent frequency selective surface in the optical range. *Opt. Express* **14,** 11945–11951 (2006).
85. De Waele, R., Burgos, S. P., Polman, A. & Atwater, H. A. Plasmon dispersion in coaxial waveguides from single-cavity optical transmission measurements. *Nano Lett.* **9,** 2832–2837 (2009).
86. Kroekenstoel, E. J. A., Verhagen, E., Walters, R. J., Kuipers, L. & Polman, A. Enhanced spontaneous emission rate in annular plasmonic nanocavities. *Appl. Phys. Lett.* **95,** 263106 (2009).
87. Pijpers, J. J. H. *et al.* Assessment of carrier-multiplication efficiency in bulk PbSe and PbS. *Nature Phys.* **5,** 811–814 (2009).
88. King, R. R. *et al.* 40% efficient metamorphic GaInP/GaInAs/Ge multijunction solar cells. *Appl. Phys. Lett.* **90,** 183516 (2007).
89. Coutts, T. J. *et al.* Critical issues in the design of polycrystalline, thin-film tandem solar cells. *Prog. Photovolt. Res. Appl.* **11,** 359–375 (2003).
90. Schuller, J. A. *et al.* Plasmonics for extreme light concentration and manipulation. *Nature Mater.* **9,** 193–204 (2010).
91. Verschuuren, M. A. & van Sprang, H. A. 3D photonic structures by sol-gel imprint lithography. *Mater. Res. Soc. Symp. Proc.* **1002,** 1002-N03-05 (2007).
92. Reilly, T., van de Lagemaat, J., Tenent, R. C., Morfa, A. J. & Rowlen, K. L. Surface-plasmon enhanced transparent electrodes in organic photovoltaics. *Appl. Phys. Lett.* **92,** 243304 (2008).
93. US Geological Survey 2004 <http://minerals.usgs.gov/minerals/pubs/mcs/>.
94. Green, M. A. Improved estimates for Te and Se availability from Cu anode slimes and recent price trends. *Prog. Phot.* **14,** 743 (2006).

Acknowledgements

We thank M. Bonn, K. Catchpole, V. E. Ferry, J. Gomez Rivas, M. Hebbink, J. N. Munday, P. Saeta, W. C. Sinke, R. E. I. Schropp, K. Tanabe, E. Verhagen, M. A. Verschuuren, R. de Waele and E. T. Yu for discussions. This work is supported by the Global Climate and Energy Project. The FOM portion of this work is part of the research programme of FOM and of the Joint Solar Panel programme, which are both financially supported by the Netherlands Organisation for Scientific Research (NWO). The Caltech portion of this work was supported by the Department of Energy under grant number DOE DE-FG02-07ER46405.

Additional information

The authors declare no competing financial interests.

CORRIGENDUM

Plasmonics for improved photovoltaic devices

Harry A. Atwater and Albert Polman

Nature Materials **9,** 205–213 (2010); published online 19 February 2010; corrected online 1 September 2010.

In Fig. 1a of the version of this Review originally published, the graph labelled '2-μm-thick Si wafer' is that for a 10-μm-thick Si wafer. The corrected figure is shown below. The original figure caption and descriptions in the text are correct. The figure has been corrected in the HTML and PDF versions of this Review.